**HEFAT2014**
**10th International Conference on Heat Transfer, Fluid Mechanics and Thermodynamics**
**14 – 16 July 2014**
**Orlando, Florida**

# ULTRASONIC MEASUREMENTS OF UNSTEADY HEAT TRANSFER IN A RECIPROCATING GAS SPRING

Richard Mathie*,[1], Alexander J. White[2], and Christos N. Markides[1]

[1] *Clean Energy Processes Laboratory, Department of Chemical Engineering*
Imperial College London, London SW7 2AZ, United Kingdom
[2] *Hopkinson Laboratory, Cambridge University Engineering Department*
Trumpington Street, Cambridge CB2 1PZ, United Kingdom

## ABSTRACT

In this paper, an experiment is reported that was devised to measure the thermodynamic loss associated with the unsteady heat transfer that takes place in the compression space of a gas spring and to differentiate the loss from any mass leakage or viscous or dissipation frictional effects. As the total mass in the system is unknown, due to leakage between the cylinder and the piston, it is necessary to measure three thermodynamic bulk parameters in order to completely determine the system state. Pressure, temperature and volume are convenient choices. However there is a challenge in measuring the gas temperature in the compression space using traditional physically invasive methods, such as thermocouples. These methods generally have a number of undesirable side effects; for example their poor response times due to the added thermal mass, their sensitivity to the varying heat transfer in the cylinder, the disruption of the gas flow and gas temperature, and the fact that they only provide a point measurement within the flow. Instead, a novel technique is presented for the estimation of the bulk temperature of the gas by measuring the time of flight of an ultrasonic pulse across the compression space. The technique is based on the principle that the speed of sound in an ideal gas is dependent on the square root of the absolute temperature, based on which the temperature of the gas along the ultrasonic path can be found. The ultrasonic pulse is transmitted and received at 400 kHz using piezo ceramic transducers with a repetition rate of 1 kHz.

This instantaneously resolved temperature information, along with the pressure and volume of the compression space, was used to calculate the work and heat flows into the compression space. It was therefore possible to measure the instantaneous rate of heat transfer throughout the compression expansion cycle of the gas spring. The heat transfer rate was seen to be linear for most of the cycle, with the heat flux proportional to the gas–wall temperature difference. There was however a deviation from this during expansion. The thermodynamic loss around the cycle of the gas spring was also measured and reported at different rotational speed. The loss was observed to increase with increasing Péclet number which was in agreement with the theoretical models of a gas spring.

*Email: r.mathie08@imperial.ac.uk, Address all correspondence to this author.

## INTRODUCTION

The efficiency of reciprocating gas compressor and expander devices is of prime importance for a number of emerging clean energy technologies, for instance Pumped Thermal Electricity Storage (PTES) [1] and Organic Rankine Cycles (ORCs) [2], as well as for more traditional uses, such as in cryogenic equipment [3]. Previous studies, such as those by Kornhauser and Smith [3] and Lekić and Kok [4] have considered the modelling and made suitable measurements of gas spring devices, since these devices remove the complex effects of gas exchange and valve timing whilst maintaining the aspects of heat transfer and gas leakage from the compression space. In Kornhauser and Smith [3] and similarly Mathie et al. [5] it was shown how the unsteady component of heat transfer contributed to the thermodynamic loss in gas springs.

## NOMENCLATURE

| | | |
|---|---|---|
| Material Properties | | |
| $c_p$ | $[\mathrm{J\,K^{-1}\,kg^{-1}}]$ | Specific heat capacity of gas at constant pressure |
| $c_v$ | $[\mathrm{J\,K^{-1}\,kg^{-1}}]$ | Specific heat capacity of gas at constant volume |
| $R$ | $[\mathrm{J\,K^{-1}\,kg^{-1}}]$ | Specific gas constant |
| $\alpha$ | $[\mathrm{m^2\,s^{-2}}]$ | Thermal diffusivity |
| $\gamma$ | [-] | Ratio of heat capacities |
| Variables | | |
| $Pe$ | [-] | Péclet number |
| $\phi$ | [-] | Phase |

| | | |
|---|---|---|
| $\psi$ | [-] | Cycle loss |
| $\dot{q}$ | [$\mathrm{W\,m^{-2}}$] | Heat flux |
| $A$ | [-] | Signal amplitude |
| $c$ | [$\mathrm{m\,s^{-1}}$] | Speed of sound |
| $D$ | [m] | Diameter of the cylinder |
| $D_h$ | [m] | Hydraulic diameter of the compression space |
| $H$ | [J] | Enthalpy |
| $m$ | [kg] | Mass of gas |
| $P$ | [$\mathrm{N\,m^{-2}}$] | Pressure |
| $Q$ | [J] | Heat |
| $S$ | [$\mathrm{m^2}$] | Surface area of compression space |
| $s$ | [-] | A signal |
| $T$ | [s] | Temperature |
| $t$ | [s] | Time |
| $V$ | [$\mathrm{m^3}$] | Volume of compression space |
| $W$ | [J] | Work |
| $\rho$ | [$\mathrm{kg\,m^{-3}}$] | Gas density |
| $\omega$ | [$\mathrm{s^{-1}}$] | Angular frequency |

| Subscripts | |
|---|---|
| 0 | At time, $t = 0$ |
| $r$ | Ratio |
| pulse | Of the pulse |
| start | At the start of the pulse |
| end | At the end of the pulse |
| ext | External |
| w | On the wall |
| gas | In the gas |
| Rx | Receiver |
| Tx | Transmitter |

| Operators | |
|---|---|
| $\mathcal{F}\{\cdot\}$ | Fourier transform |
| $(\cdot)^*$ | Complex conjugate |

In the present paper, an experiment is devised to measure the thermodynamic loss associated with the unsteady heat transfer that takes place in the compression space of a gas spring and differentiate the loss from any mass leakage or viscous or dissipation frictional effects. As the total mass in the system is unknown, due to leakage between the cylinder and the piston, it is necessary to measure three thermodynamic bulk parameters in order to completely determine the system state. Pressure, temperature and volume are convenient choices. However there is a challenge in measuring the gas temperature in the compression space using traditional physically invasive methods, such as thermocouples. These methods generally have a number of undesirable side effects; for example their poor response times due to the added thermal mass, their sensitivity to the varying heat transfer in the cylinder, the disruption of the gas flow and gas temperature, and the fact that they only provide a point measurement of the flow.

For an ideal gas the speed of sound is given by,

$$c_{\mathrm{gas}} = \sqrt{\gamma R T}\,, \tag{1}$$

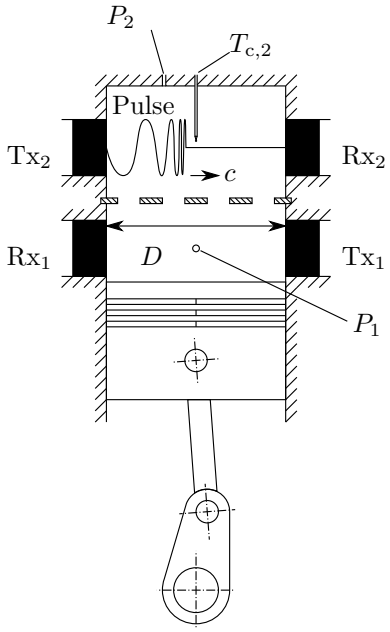


Figure 1: A schematic of the gas spring arrangement.

where $R$ is the mass specific gas constant and,

$$\gamma = \frac{c_p}{c_v}\,, \tag{2}$$

is the heat capacity ratio of the gas. Typically for air $\gamma = 1.4$ and $R = 287\ \mathrm{J\,K^{-1}\,kg^{-1}}$. It is proposed here that by timing the transit of an ultrasonic pulse across the compression space the temperature of the compression space can be deduced.

## EXPERIMENTAL METHODS

A custom compression space was fitted to the cylinder head of a commercially sourced compressor to form a gas spring system (see Fig. 1). The compressor has a bore, $D$, of 105 mm and a stroke length of 78 mm and was rated to 1500 rpm and a maximum pressure of 10 bar. The locations of the pressure measurements thermocouples and ultrasonic transmitters and

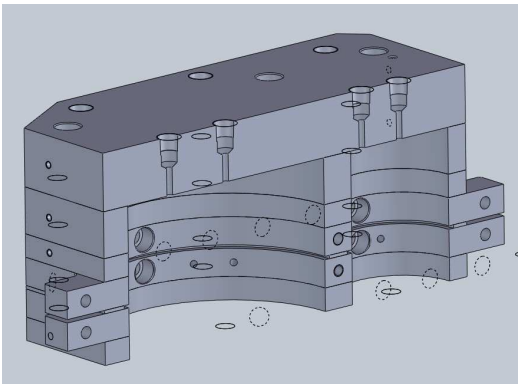

Figure 2: CAD model of the compression space for the gas spring to replace the original cylinder head of the compressor.

receivers are shown in Fig. 1. The compression space has a moulder construction allowing different test sections and spacers to be added to change the compression ratio. An optional baffle can be placed between the upper and lower segments of the compression space to investigate the effect of orifice induced turbulence on the heat transfer in the gas spring. However, only a single chamber compression space will be investigated here. For the initial experiment the size of the compression space was 14 mm resulting in a theoretical isentropic pressure ratio, $P_r$, of 13.7.

The compressor was belt driven by an 11 kW induction motor with a reduction ratio of about 2:1 between the pulleys. The motor was powered using a Mitsubishi FR-E740 3–phase inverter which gave a great degree of controllability over the rotation speed of the compressor.

In this paper a novel technique is presented for the measuring of the temperature of the gas by measuring the time of flight of an ultrasonic pulse across the compression space. The technique is based on the principal that the speed of sound in an ideal gas is dependent on the square root of the absolute temperature, based on which the temperature of the gas along the ultrasonic path can be found. The ultrasonic pulse is transmitted and received at 400 kHz using piezo ceramic transducers with a repetition rate of 1 kHz. The results are compared to that obtained with a fine 0.075 mm K-type thermocouple and the relative accuracy of the two techniques are evaluated with increasing operational frequency. The temperature measurements of the gas space along with the measured gas pressure and volume of the gas space are then used to infer the instantaneous mass and heat transfer out of the volume, and thus to evaluate the thermodynamic losses.

## Ultrasonic temperature measurements

To measure the time of flight across the compression space two 10 mm diameter ultrasonic transducers were glued into reassesses in the walls of the compression space ring Fig. 2.

The signal for the transmitting transducer (Tx) was output from digital to analog converter (DAC) of the Agilent U2531 with a resolution of 12-bits, and a sample rate of 1 MHz as shown in Fig. 3. A wideband amplifier with a maximum output of 30 volt peak to peak and an output impedance of 50 Ω and a band pass up to 1 MHz was used to drive the transmitting transducer.

The ultrasonic pulse generated by the transmitting transducer travels across the compression space, Fig. 2, and after a short delay, related to the gas temperature in the compression space, is picked up by the receiving transducer. The output from the receiving transducer is very small, of the order of µV, and has a high impedance. In order to minimise the noise picked up and to prevent loading the transducer with the line impedance, resulting in a reduced signal and frequency response, a pre-amplification stage with a gain of 100 is used close to the transducer (see Fig. 3). The pre–amp

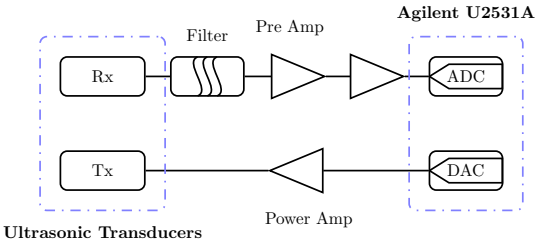


Figure 3: Amplification and filter arrangement between the transmitting (Tx) and receiving (Rx) transducers and the digitiser.

stage used was a simple non inverting op-amp design using an LT1222 amp. The LT1222 was used due to its low input noise of 3 nV $\mathrm{Hz}^{-0.5}$ and high gain bandwidth product of 500 MHz which was needed to achieve sufficient bandwidth.

Another stage of amplification gets the signal in to the range for sampling by the 14-bit ADC of the U2531 digitiser. The digitised signal is then sent to the a computer for further processing.

### Pulse compression

A signal processing technique called pulse compression is often employed in sonar, radar and other echo–graphic methods to improve the signal to noise ratio and range resolution of the measurement [6]. This improvement is achieved by modulating the transmitted signal and then correlating the received signal with the transmitted signal. To understand how this is achieved first considering a sinusoidal signal with no modulation,

$$s(t) = \begin{cases} A \sin 2\pi f_0 t & \text{if } 0 \le t < t_{\text{pulse}} \\ 0 & \text{otherwise.} \end{cases} \tag{3}$$

The range resolution of a signal is dictated by the ability to discern separate received signals. In the case of the unmodulated signal in (3) if two retuning signals arrive at nearly the same time the two signals will become mixed and it will be impossible to separate them. The range resolution is therefore half of the time period of the pulse or $\frac{1}{2}ct_{\text{pulse}}$. This means a shorter pulse will give better range resolution.

On the other hand the energy transmitted by the transducer will be,

$$E = \int_0^{t_{\text{pulse}}} s^2(t)dt = A^2 t_{\text{pulse}}\,, \tag{4}$$

and the energy of the received signal will be a scaled by the channel response $E_{\text{Rx}} = K^2 A^2 t_{\text{pulse}}$. Hence if the channel noise is characterised by its standard deviation, $\sigma$, then the signal to noise ratio is,

$$\text{SNR} = \frac{K^2 A^2 t_{\text{pulse}}}{\sigma^2}\,. \tag{5}$$

Here the signal to noise ratio is improved by a longer signal pulse. This resulting trade off between range

resolution and signal to noise ratio is addressed by the pulse compression technique.

What is needed is a signal with a wide spectrum bandwidth, like the delta function, allowing fine resolution of the received signal, but with the energy content spread over a larger period of time. One such signal is a linear frequency sweep or "chirp". This pulse will start at starting frequency $\omega_{\text{start}}$ and ends at $\omega_{\text{end}}$ and has a duration of $t_{\text{pulse}}$,

$$\omega(t) = \omega_{\text{start}} + (\omega_{\text{end}} - \omega_{\text{start}})\frac{t}{t_{\text{pulse}}}\,. \tag{6}$$

The angular frequency of a signal is by definition the derivative of the phase of a signal and so the signal phase can be found by integration,

$$\begin{aligned}\phi(t) &= \int_0^t \omega(\tau)d\tau \\ &= \omega_{\text{start}}t + (\omega_{\text{end}} - \omega_{\text{start}})\frac{t^2}{2t_{\text{pulse}}}\,. \end{aligned}\tag{7}$$

Therefore the transmitted signal is,

$$s_{\text{Tx}}(t) = \begin{cases} A\sin\phi(t) & \text{if } 0 \le t < t_{\text{pulse}} \\ 0 & \text{otherwise.} \end{cases} \tag{8}$$

The pulse can be recovered by calculating the cross correlation between the transmitted Tx and received, Rx, signals,

$$s_{\text{Rx}} \star s_{\text{Tx}} = \int_{-\infty}^{\infty} s_{\text{Rx}}(t)s_{\text{Tx}}(t+\tau)d\tau\,. \tag{9}$$

The result will be equal to the autocorrelation of the transmitted signal $s_{\text{Tx}}$ convolved with the channel response denoted $G(z)$. Neglecting the channel response for now it can be seen that the autocorrelation of $s_{\text{Tx}}$ will take the form,

$$\begin{aligned} &s_{\text{Tx}} \star s_{\text{Tx}} = \\ &A^2 t_{\text{pulse}}\Lambda\left(\frac{t}{t_{\text{pulse}}}\right)\text{sinc}\left\{\Delta\omega\Lambda\left(\frac{t}{t_{\text{pulse}}}\right)\right\}\sin\omega_0 t\,, \end{aligned}\tag{10}$$

where $\Lambda(\cdot)$ is the triangle function

$$\Lambda(x) = \begin{cases} 1+2x & -\frac{1}{2} \le x < 0 \\ 1-2x & 0 \le x < \frac{1}{2} \\ 0 & \text{otherwise.} \end{cases} \tag{11}$$

The cardinal sine function, seen in Eq. 10, has a $-3$dB temporal width of approximately $t' = 2\pi/\Delta\omega$. Hence after calculating the cross correlation of the transmitted signal chirp with the received signal the spatial resolution becomes $\pi c/\Delta\omega$. The pulse has effectively been compressed by the ratio $t_{\text{pulse}}\Delta f$ hence the name pulse compression. In a similar manor the power of the signal after pulse compression can be considered to be amplified by $t_{\text{pulse}}\Delta f$ hence the signal to noise ratio becomes,

$$\text{SNR} = \frac{K^2A^2t_{\text{pulse}}^2\Delta f}{\sigma^2}\,. \tag{12}$$

In the case of the experiment it is more computationally efficient to calculate the cross correlation using a fast Fourier transform (fft) than directly computing the correlation. This technique takes advantage of convolution theorem such that,

$$\mathcal{F}\left\{s_{\text{Rx}} \star s_{\text{Tx}}\right\} = \mathcal{F}\left\{s_{\text{Rx}}\right\}\left(\mathcal{F}\left\{s_{\text{Tx}}\right\}\right)^*\,, \tag{13}$$

where $\mathcal{F}\{\cdot\}$ denotes the Fourier transform and $(\cdot)^*$ denotes the complex conjugate. Strictly speaking this is for a circular convolution however this method remains valid as long as the signal is reasonably periodic from sample window to sample window or if the received signal is more than the pulse length from the end of the sample window.

For the current experiment the frequency sweep went from 310 kHz to 370 kHz with a pulse length, $t_{\text{pulse}}$, of 128 µs and a repetition rate of 500 µs, i.e. 2000 Hz. This gives a bandwidth of 60 kHz which results in a pulse compression ratio of 7.7 and range resolution of between 4 and 8 mm.

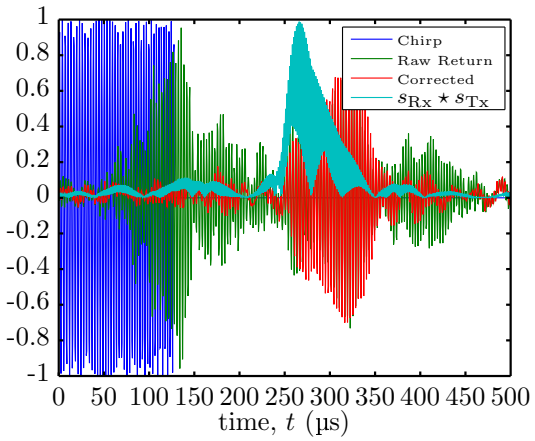


(a) Strong return when near TDC.

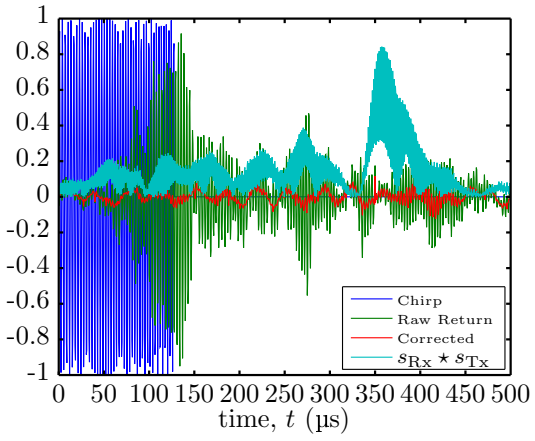


(b) Weak return when near BDC.

Figure 4: Examples of typical ultrasonic transmissions across the compression space.

#### Temperature calculation

The time of flight for the pulse across the compression space can be found by,

$$t_{\text{flight}} = \arg\max_t\left(s_{\text{Rx}}(t) \star s_{\text{Tx}}(t)\right)\,. \tag{14}$$

For an ideal gas the temperature can be found from,

$$c = \frac{D}{t_{\text{flight}}} = \sqrt{\gamma R T_{\text{gas}}}\,. \tag{15}$$

Rearranging gives a measure of the gas temperature,

$$T_{\text{gas}} = \frac{1}{\gamma R}\left(\frac{D}{t_{\text{flight}}}\right)^2. \tag{16}$$

This temperature measurement has a contribution from every location along the path between the two transducers. However this temperature measurement is not a straight forward line mean or volumetric average temperature. Consider that the time of flight for the pulse can also be written as,

$$t_{\text{flight}} = \int_0^D \frac{1}{\sqrt{\gamma R T(x)}} dx\,. \tag{17}$$

Using Eq. 16, the measured gas temperature is therefore,

$$T_{\text{gas}} = \left(\frac{D}{\int_0^D \frac{1}{\sqrt{T(x)}} dx}\right)^2. \tag{18}$$

This is quite a complex relation, however as long as $T(x)$ is reasonable uniform $T_{\text{gas}}$ should remain a good approximation to the volumetric mean temperature along the measurement line.

## RESULTS AND DISCUSSION

An example of the transmitted and received signals is shown in Fig. 4. Transmission and recording of the signals were synced so that 1000 samples were read in by the digitiser ADC as 500 samples were converted by the DAC. The difference in the number of samples recorded or transmitted per frame is due to the maximum sample rate of the ADC (2 Ms/s) and DAC (1 Ms/s)of the digitiser. The transmitted "chirp", $s_{\text{Tx}}$, can be seen in blue at the start of the sampled frame and the captured ping, $s_{\text{Rx}}$, is shown in green. A correction is made to account for the sound travelling around the solid compression block, as described later, and is shown in red. The cross correlation of the transmitted signal with the corrected received signal is also shown in light blue. The position of peak magnitude of the cross correlation gives the time delay of the signal.

### Signal processing

The plots in Fig. 4 show that there is a strong return, in the raw signal, starting 30 µs. This was due to a flaw in construction in which the transmitting transducer was glued too firmly into the compression space resulting in poor isolation. This resulted in a large proportion of the sound being conducted through the aluminium head block around the perimeter of the compression space. To check this is the case, consider that at room temperature the longitudinal speed of sound in aluminium is 6420 $\text{m}\,\text{s}^{-1}$ and the path length around the perimeter from transducer to transducer is $\pi 105/2$ mm which equates to a delay time of 26 µs. This is consistent with the estimate from the plots in Fig. 4 and is a lower bound estimate on the delay time for the transmission of sound through the aluminium head block. In reality the path length would be a little longer as the perimeter is the the smallest possible path.

The erroneous signal, due to the transmission of ultrasound around the compression space through the solid head block, and the subsequent echoes, proves to problematic as it is impossible to distinguish it from the signal transmitted across the compression space, through the gas. In Fig. 5a an image is made of the raw returned signals such that each frame or "scan" makes up a column of the image. Subsequently the horizontal axis "Scans" represents time and vertical "Samples" axis corresponds to the delay of the received signal from the pulse. The erroneous signal from the transmission around the solid head block can be seen as a horizontal streak in Fig. 5a between the 200 and 300 samples mark. The main transmission across the compression space can also be seen Fig. 5a but is only clearly visible at periodic intervals between the 500 and 600 sample mark. This periodic strengthening of the signal corresponds to when the piston is near top dead centre and so the gas in the compression space is at its densest. That is gas with a higher density gives a strong coupling between the transducers resulting in a large received signal.

Fortunately the erroneous signal is constant throughout the cycle, whereas the required signal moves with the changing gas temperature. As it it unlikely that the gas temperature will be correlated to the signal, by taking the mean of all the scans an average trace of the erroneous signal can be made. That is as the delay times of the desired signals are not correlated averaging them should result in zero. Then by subtracting this average from the recorded scans the desired signal can be recovered. Figure 5b shows the signal with the average subtracted. The erroneous signal is now completely removed and the transmission across the compression space can be seen more clearly.

Finally the cross correlation is taken and the delay of the signal is identified, as shown in 5c. It can be seen how the delay time varies periodically as the piston moves from TDC to BDC. Both Fig. 5c and 6 show images of the cross correlation and the resulting peak signal. At bottom dead centre the gas density lowers reducing the received signal. The increase in relative noise can be seen in Fig. 5c where the scans have been scaled by the the peak correlation. Also in both figures more scatter is seen at bottom dead centre of the measured delay. Filtering was then applied to remove the glitches and noise in the delay measurement.

In Fig. 7 the pressure, temperature and gas density in the compression space at 330 rpm is shown. The figures for temperature, Fig. 7a and density, Fig. 7c, which incorporate the time of flight data have been processed with a bivariate histogram to show the data

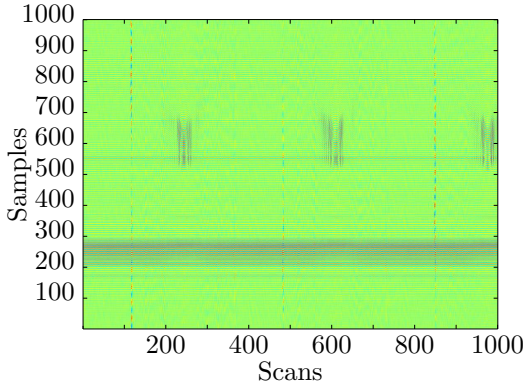


(a) Raw ultrasonic return signal arranged in blocks of scans.

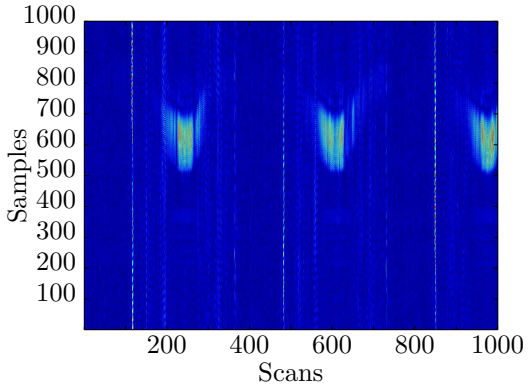


(b) Return minus the mean return signal.

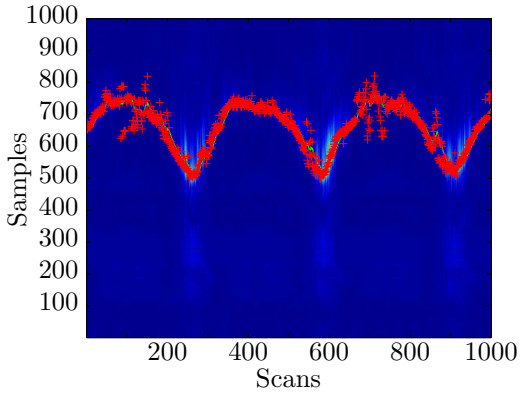


(c) Output of cross correlation. The index of the peak value is shown and indicates the signal delay.

Figure 5: Processing steps of the Ultrasonic data, with the gas spring operating at 330 rpm and the pressure oscillating between 1 and 7 bar.

more clearly. It can be seen that for this case the measured gas temperature oscillates between 200 and 400 K during a cycle. Interestingly that the peak pressure is reached at top dead centre, $\psi = \frac{3}{2}\pi \approx 4.7$, but the peak temperature occurs significantly before that point at $\psi \approx 4$. This shows that significant heat transfer is taking place during a cycle.

### Parameter measurements in the gas spring cycle

As the bulk temperature of the gas can now be estimated from the time of flight measurements the bulk

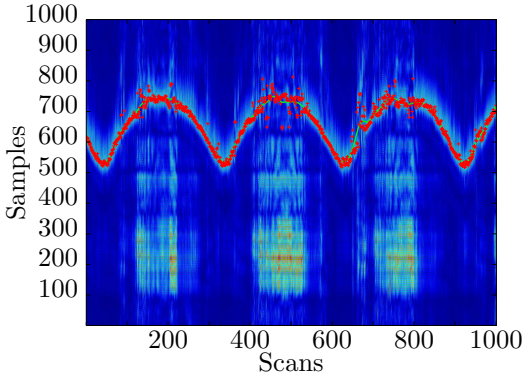


Figure 6: Another example of the cross correlation of the received signal at 400 rpm with each scan normalised by the maximum correlation for that scan.

gas density can be calculated by,

$$\rho_{\text{gas}} = \frac{P}{RT_{\text{gas}}} \,. \tag{19}$$

The total mass of gas in the compression space can therefore be found as

$$m = \rho_{\text{gas}} V \,. \tag{20}$$

This allows the gas leakage around the piston rings to be accounted for. The mass loss can be found by differentiation,

$$\dot{m} = \frac{\partial m}{\partial t} \,. \tag{21}$$

However signal processing techniques must be used to account for measurment noise.

The work done on the volume can be calculated simply from the measured pressure and displacement of the piston,

$$\dot{W} = P\frac{\partial V}{\partial t} \,. \tag{22}$$

The rate of heat exchange through the walls of the cylinder and piston can be calculated by using the 1$^{\text{st}}$ law,

$$\dot{Q} = \dot{H} - V\frac{\partial P}{\partial t} + \dot{H}_{\text{flow}} \,. \tag{23}$$

The enthalpy form of the 1$^{\text{st}}$ law is used as it is better suited for a control volumes where there is mass exchange. Here the enthalpy of the gas inside the compression space can be estimated from the measured gas temperature by,

$$H = mc_pT_{\text{gas}} \,, \tag{24}$$

where the mass in the compression space $m$ was calculated in Eq. 21.

The enthalpy flow in or out of the cylinder due to leakage depends on the direction of mass transfer, and is estimated by,

$$\dot{H}_{\text{flow}} = \begin{cases} c_pT_{\text{ext}}\dot{m} & \text{if } \dot{m} > 0 \\ c_pT_{\text{gas}}\dot{m} & \text{if } \dot{m} < 0 \,. \end{cases} \tag{25}$$

That is, if mass is being lost from the compression space then the enthalpy of that gas stream can be

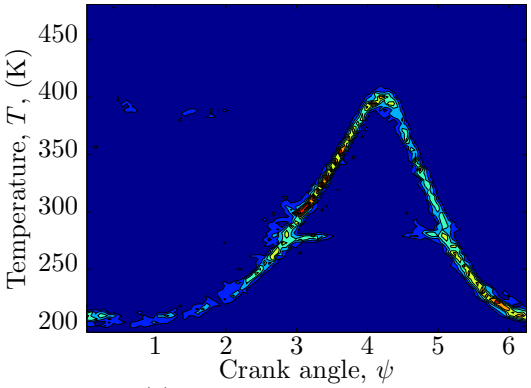


(a) Gas temperature $T_{\text{gas}}$.

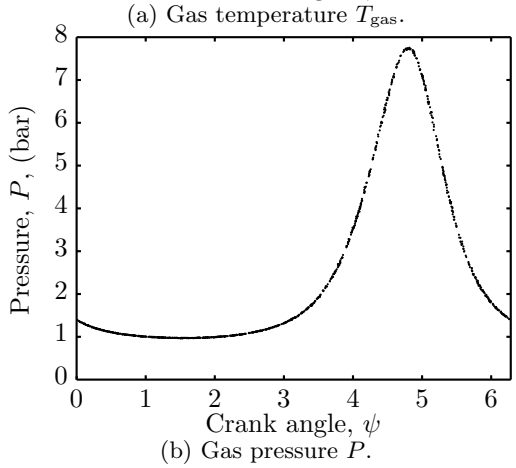


(b) Gas pressure $P$.

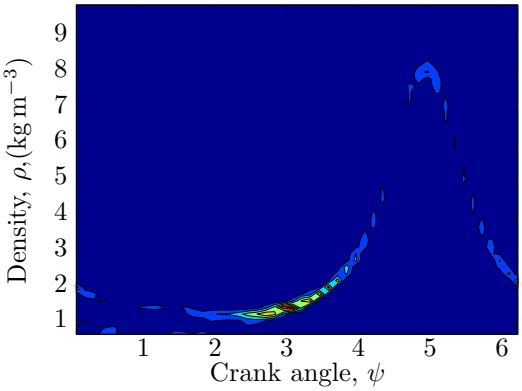


(c) Gas density $\rho$.

Figure 7: Gas density, pressure and temperature in the compression space through a cycle at 330 rpm.

estimated based on the gas temperature in the compression space. Similarly if mass is transfers back into the compression space the enthalpy of the flow can be estimated based on the external gas temperature, the temperature of the gas inside the crank case in this instance.

### Heat transfer estimation

From Eq. 23 the heat transfer rate and wall heat flux can be estimated. The total heating rate against crank angle for a number of cycles is shown in Fig. 8. A negative heat rate shows that heat is leaving the system and a positive heat rate shows heat entering the system. It can be seen how the minimum heat rate occurs at the point where the gas temperature is highest, $\psi \approx 4$. The heat rate then passes through zero around top dead centre and is positive through most of the expansion.

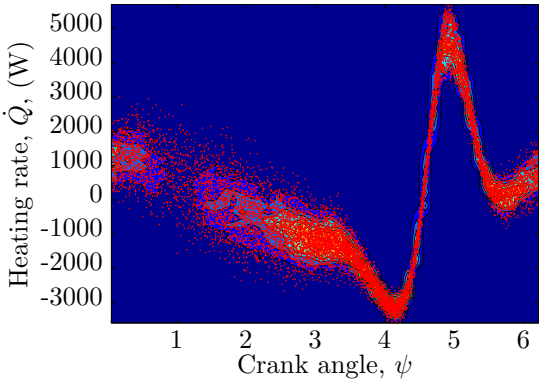


Figure 8: Heat rate through the cycle at 330 rpm.

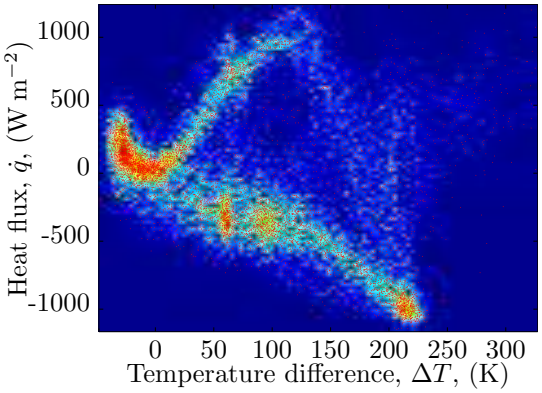


Figure 9: Heat flux against gas–wall temperature difference, $\Delta T$, at 330 rpm.

A plot is shown in Fig. 9 of the wall heat flux,

$$\dot{q} = \frac{\dot{Q}}{S_{\text{w}}}\,, \tag{26}$$

against the temperature difference between the bulk of the gas and the wall, $\Delta T = T_{\text{gas}} - T_{\text{w}}$. Here $S_{\text{w}}$ is the total wall surface area inside the compression space. It can be seen that the relationship between $\Delta T$ and heat flux, $\dot{q}$, is predominantly liner with a slope approximately -5. That is, a heat transfer coefficient of 5 W m$^{-2}$ K$^{-1}$. However there is a large deviation from this, which occurs during expansion, whereby a positive heat flux is seen despite the temperature of the gas being higher than the wall. This has been explained by Lee et al. [3, 7, 8] and is due to the unsteady conduction of heat through the air in the compression space. Effectively there is a small layer of air, a thermal boundary layer, which is in contact with the wall and has a non uniform temperature profile due to unsteady heat transfer. This can result in an inversion in the overall heat flux into the compression space despite the total temperature difference between the bulk gas temperature and wall temperature being positive.

### Cycle loss

The pressure–volume diagram for the gas spring operating at 330 rpm is shown in Fig. 10. It can be seen

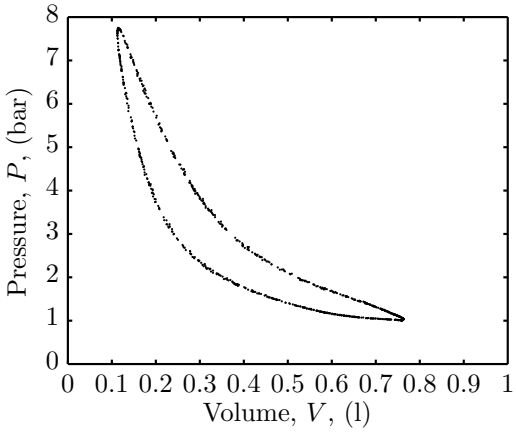

Figure 10: $P$–$V$ cycle diagram at 330 rpm.

how the pressure lags behind the volume slightly due to the heat transferred during the cycle. The area enclosed by the loop represents the work done to make the gas spring complete one cycle.

The work done during one cycle can be normalised by the total compression expansion work done by the gas spring,

$$\psi = \frac{\oint P\partial V}{\oint |P\partial V|}\,. \tag{27}$$

This represents the average loss during compression and expansion of the gas spring. Figure 11a shows the measured loss for this experiment against the Péclet number. Here the Péclet number represents a dimensionless rotation speed,

$$Pe = \frac{D_h^2\omega}{4\alpha_{\text{gas}}}\,, \tag{28}$$

where $\alpha_{\text{gas}}$ is the thermal diffusivity of the gas and $D_h$ is the effective hydraulic diameter of the compression space. Here the effective hydraulic diameter is

$$D_h = \frac{V_0}{S_{\text{w},0}}\,, \tag{29}$$

where $V_0$ is the volume of the compression space, and $S_{\text{w},0}$ is the surface area of the inside of the compression space with the piston at mid-stroke.

It can be seen that the loss shown in Fig. 11a is increasing with Péclet number. A similar pattern is observed in Fig. 11b from Mathie et al. [5] and similar studies [3, 4, 7, 8]. There, it was shown that at low rotational speed the cycle loss is low as the gas spring is behaving in an isothermal manner. However, as the speed is increased the losses increase as the gas spring departs from the isothermal ideal. In theory at even higher speeds the loss should drop again as the gas spring approaches the adiabatic ideal.

In the experiment shown here however the higher speeds needed to reach this regime could not be attained due to a problem in the mechanical arrangement leading to unwanted vibrations. Also the increase in loss for the gas spring occurs later, at higher $Pe$, in the experiment than in the theory. This could be the

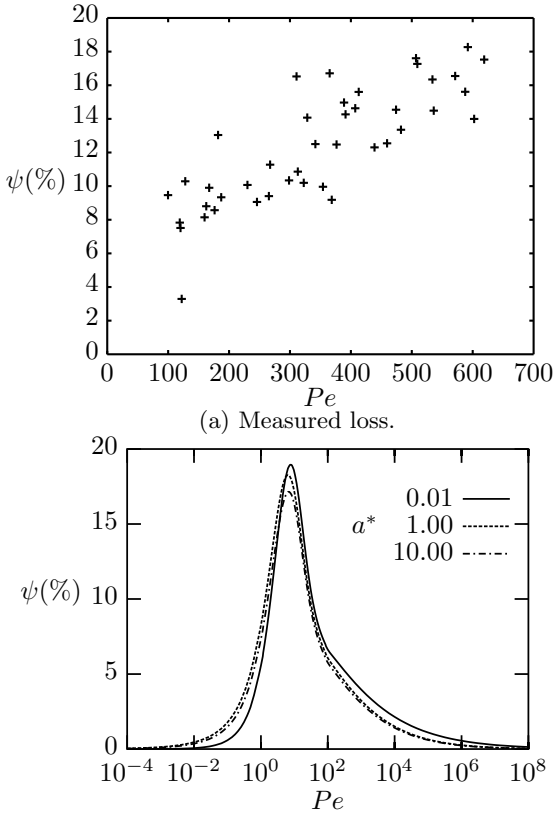

(a) Measured loss.

(b) Theoretical loss from Mathie et al. [5].

Figure 11: Cycle loss, $\psi$, against Péclet number, $Pe$.

result of a number of effects; Firstly the mass leakage from the piston seals, and secondly an increase in the effective thermal diffusivity due to extra turbulent mixing in the compression space. Additional refinements will have to be made to the experiment to address these problems and improve the observations. However for this preliminary study it has been shown that the ultrasonic technique described is capable of producing accurate repeatable non invasive measurements of the gas temperature with very fast response times.

## CONCLUSION

A novel non invasive technique was devised to measure the gas temperature in the compression space of a reciprocating device, specifically a gas spring. The technique was able to measure the compression space temperature with a high degree of accuracy and with a fast response time. Using this information it was possible to compensate for gas exchange around the piston and piston rings. This made it possible to measure the instantaneous rate of heat transfer within the cylinder.

The heat transfer rate was seen to be linear for most of the cycle, with the heat flux proportional to the gas–wall temperature difference. However there was a large transient from this linear behaviour when the piston reached top dead centre. At this point a reversal in the heat flux was seen despite the wall temperature being lower than the gas. This behaviour is predicted by theory and is due to the temperature of the layer of gas in contact with the wall falling below the wall and

bulk temperatures during expansion.

The thermodynamic loss around the simple compression expansion cycle of the gas spring was also measured and reported at different rotational speed. The observed increase in cycle loss with increasing Péclet number was in agreement with the theoretical models of the gas spring. However the current experiment was not able to reaches the higher speeds needed to see the loss drop again when the gas spring reaches the adiabatic regime.

## REFERENCES


[1] White A., Parks G., and Markides C.N., Thermodynamic analysis of pumped thermal electricity storage, *Applied Thermal Engineering*, Vol. 53, 2012, pp. 291-298

[2] Wronski J., Skovrup M.J., Elmegaard B., Rislå H.N., and Haglind F., Design and modelling of a novel compact power cycle for low temperature heat sources, *Proceedings of the 25$^{th}$ International Conference on Efficiency, Cost, Optimization, Simulation and Environmental Impact of Energy (ECOS)*, 2012

[3] Kornhauser A.A., and Smith J.L., Heat transfer with oscillating pressure and oscillating flow, *Proceedings of the 24$^{th}$ I.E.E.E. Intersociety Energy Conversion Engineering Conference*, 1989, pp. 2347-2353

[4] Lekić U., and Kok. J.B.W., Heat transfer and fluid flows in gas springs, *Open Thermodynamics Journal*, Vol. 4, 2010

[5] Mathie R., Markides C.N., and White A., A framework for the analysis of thermal losses in reciprocating compressors and expanders, *Heat Transfer Engineering*, Vol. 34, 2014, pp. 1435-1449

[6] Klauder J.R., Price A.C., Darlington S., and Albersheim W.J., The theory and design of chirp radars, *Bell System Technical Journal*, Vol. 39, 1960, pp. 745–808

[7] Lee K.P., A simplistic model of cyclic heat transfer phenomena in closed spaces, In *Proceedings of the 18$^{th}$ Intersociety Energy Conversion Engineering Conference (IECEC'83)*, Vol. 1, 1983, pp. 720-723

[8] Kornhauser A.A., and Smith J.L., Application of a complex nusselt number to heat transfer during compression and expansion, *Journal of Heat Transfer*, Vol. 116, 1994, pp. 536–542